Materials Science and Engineering A 535 (2012) 22–31

Contents lists available at SciVerse ScienceDirect

Materials Science and Engineering A

journal homepage: www.elsevier.com/locate/msea

The effects of Ti and Sn alloying elements on precipitation strengthened Cu40Zn brass using powder metallurgy and hot extrusion

Shufeng Li[a,*], Hisashi Imai[a], Haruhiko Atsumi[a], Katsuyoshi Kondoh[a], Akimichi Kojima[b], Yoshiharu Kosaka[b], Koji Yamamoto[c], Motoi Takahashi[c]

[a] Joining and Welding Research Institute, Osaka University, Japan
[b] San-Etsu metals Co. Ltd., 1892, OHTA, Tonami, Toyama, Japan
[c] Nippon Atomized Metal Powders Corporation, 87-16, Nishi-Sangao, Noda, Chiba, Japan

ARTICLE INFO

Article history:
Received 20 September 2011
Received in revised form
12 December 2011
Accepted 13 December 2011
Available online 21 December 2011

Keywords:
Brass
Spark plasma sintering
Powder metallurgy
Extrusion
Precipitation strengthening
Solid solution
Mechanical property
Phase transformation

ABSTRACT

The effects of Ti and Sn alloying elements on the microstructural and mechanical properties of 60/40 brass were studied by powder metallurgy processing. The super-saturated solid solution of Ti creates a high precipitation reaction chemical potential in water-atomized BS40-1.0Ti brass powder. Consequently, BS40–1.0Ti brass was remarkably strengthened by the addition of Ti. However, Ti readily segregated in the primary particle boundaries at elevated temperatures, which detrimentally affected the mechanical properties of BS40–1.0Ti brass. Accordingly, Sn was proposed as an additive to BS40–0.6Sn1.0Ti to inhibit the segregation of Ti. Consequently, the Ti precipitate was retained in the form of $CuSn_3Ti_5$ in the interior of grains and grain boundaries rather than in the primary particle boundaries. This result demonstrates that the addition of Sn can effectively hinder Ti segregation in the primary particle boundaries. Sn addition produced significant grain refinement and mechanical strengthening effects in BS40–0.6Sn1.0Ti brass. As a result, outstanding strengthening effects were observed for BS40–0.6Sn1.0Ti sintered at 600 °C, which exhibited a yield strength of 315 MPa, an ultimate tensile strength of 598 MPa, and a Vickers microhardness of 216 Hv. These values represent increases of 27.5%, 20.1% and 45.6%, over those of extruded BS40–1.0Ti brass.

1. Introduction

Brasses are by far the most commonly cast copper alloys. Because of their excellent castability, relatively low cost, and favorable combination of strength and corrosion resistance, cast brasses are extensively used in many applications [1–3]. The widely used α + β brasses exhibit the best combination of high technological and service properties. Solid-solution strengthening and precipitation hardening are the primary methods used for the development of high-strength brasses. These effects are achieved by the introduction of alloying elements and impurities to improve the mechanical properties of α + β brasses [4–6].

The binary phase diagrams of copper alloys [7] show that Cr, Fe, Ti, Zr, Mg, Sn, etc. can serve as candidate alloying elements for precipitation strengthening to develop high-strength copper alloys because the solid solubility of these alloying elements in copper decreases sharply with decreasing temperature. Titanium is virtually insoluble in copper, and concentrations in excess of 0.2 wt% of Ti can induce precipitation. The phase diagram shows five intermediate phases in the Cu–Ti system [8]: Cu_4Ti, Cu_3Ti_2, Cu_4Ti_3, CuTi and $CuTi_2$. The existence of such a large number of phases suggests Ti as an attractive candidate element that may be expected to develop high-strength brasses by precipitation hardening.

Powder metallurgy (P/M) techniques are more flexible than casting and forging techniques, allowing the fabrication of components that would otherwise decompose or disintegrate in the direct alloying of fused materials [9]. Rapid solidification (i.e., a high cooling rate) can lead to a super-saturated Ti solid solution in a brass matrix. Upon heat treatment, very fine dispersoids of the second phase are precipitated in the matrix; as a result, the precipitation hardening effect is greatly intensified. Our previous study [10,11] involved the addition of Ti to 60/40 brass, which favored grain refinement by increasing the formation rate of nucleation and recrystallization centers and by retarding the subsequent grain growth by fine precipitates. When dissolved in the super-saturated α solid solution and the β phase, Ti increases the ultimate tensile strength, the yield strength and the hardness; it also affects the phase-transformation temperature. Unfortunately, precipitation strengthening effects in the alloys produced by the powder

* Corresponding author at: 11-1, Mihogaoka, Ibaraki, Osaka 567-0047, Japan. Tel.: +81 6 6879 8669; fax: +81 6 6879 8669.
E-mail address: shufenglimail@gmail.com (S. Li).

0921-5093/$ – see front matter © 2011 Elsevier B.V. All rights reserved.
doi:10.1016/j.msea.2011.12.036

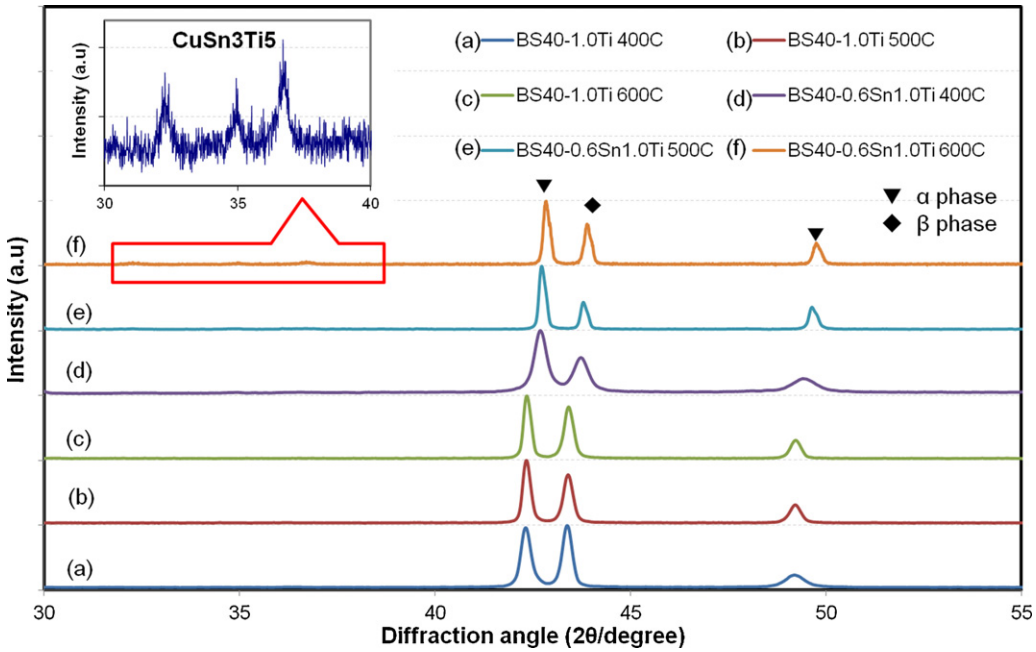

Fig. 1. X-ray diffractograms of the BS40–1.0Ti and BS40–0.6Sn1.0Ti raw powder and SPS compacts that were prepared at different temperatures in the range of 400–600 °C.

metallurgy route weaken continuously with increased processing temperature because of the segregation and coarsening of the Ti precipitates in the primary particle boundaries.

The development of systematic knowledge related to the thermo-dynamic precipitation of Ti in brasses is necessary to investigate the feasibility of developing new high-strength brasses with the combination of the properties obtained from the precipitation–hardening response of Ti to powder metallurgy processing. In this study, Sn was proposed as an additive for the Cu40Zn–1.0 wt% Ti brass for the alloy designation and processing method. As a conventional alloying additive for copper alloys, Sn is completely soluble in copper. It also forms solid solutions with copper that can significantly increase the strength and corrosion resistance of the resulting alloys. Alternatively, the interactions of the binary Cu–Ti [12–14], Ti–Sn [15] and Cu–Sn [16] systems as well those of the ternary Cu–Ti–Sn system [17,18] are an interesting topic with respect to the possibility of joining materials by the transition liquid-phase method. The introduction of Sn to brass is expected to impede the segregation of Ti and to stabilize the mechanical properties of Ti brass during powder metallurgy processing at high temperatures. The microstructure, phase transformation, precipitation behavior and mechanical properties of the 60/40 brass with Ti and Sn alloying elements as pre-alloyed P/M materials are investigated in detail.

2. Experimental methods

Water-atomized BS40, BS40–1.0Ti and BS40–0.6Sn1.0Ti pre-alloyed powders (Nippon Atomized Metal Powders, Japan) were used as the raw materials in the as-received state. The chemical compositions of the raw powders are shown in Table 1. For sintering, the raw powder was loaded into a cylindrical graphite die and consolidated by spark plasma sintering (DR.Sinter/SPS-1030; Sumitomo Coal Mining, Japan); sintering temperatures from 400 °C to 600 °C were used, with an interval of 100 °C. After holding at the desired temperature for 1.8 ks at pressure of 40 MPa, the sample was cooled in the chamber to less than 150 °C. The resulting sintered billets with diameters of 41 mm were preheated to 650 °C for 1.8 ks under a nitrogen gas atmosphere. They were then extruded using a hydraulic press with a load of 2000 kN (SHP-200-450; Shibayama Machine, Japan). The final diameter after extrusion was 7 mm. The extruded round bar was machined into test samples with diameters of 3 mm, in accordance with ICS 59.100.01. Tensile tests were conducted on a universal testing machine (Autograph AG-X 50 kN; Shimadzu, Japan) with a strain rate of $5 \times 10^{-4}\,s^{-1}$. The strain was recorded using a CCD camera accessorized to the machine. Three samples were prepared under identical conditions for the tensile strength tests to obtain the average value. The micro-hardness was measured by a Vickers micro-hardness tester (HMV-2T; Shimadzu, Japan); 30 measurements were conducted to obtain an average value.

The phase compositions of the samples were identified using X-ray diffraction (Labx, XRD-6100; Shimadzu, Japan). The measured spectra were compared to the standard ICDD PDF cards available in the system software. The microstructural evaluations of the park plasma sintering(SPS)-compacts and extruded samples were conducted using a field-emission scanning electron microscope (FE–SEM, JEM-6500F; JEOL, Japan) and a transmission electron microscope (TEM; JEM-3010, JEOL, Japan). The phases were examined using an energy-dispersive X-ray spectrometer (EDS) attached to the SEM. The crystal orientation information, which also contained grain size and phase information, was analyzed using the electron backscatter diffraction (EBSD) technique. EBSD was performed using a TSL (TSL DigiView IV; EDAX, USA) instrument attached to the FE-SEM, which was operated at 20 kV. The longitudinal cross-sections of the extruded samples were mechanically ground to a 5 μm silicon-carbide paper finish and vibratory polished for 30 min to remove any remaining surface damage. The

Table 1
Particle size and chemical compositions of the BS40, BS40–1.0Ti and BS40–0.6Sn1.0Ti alloy powders.

Powders	Particle size (μm)		wt%				
	Median size	Mean size	Zn	Ti	Sn	O	Cu
BS40	248	279	40.00	–	–	0.05	Bal.
BS40–1.0Ti	206	250	41.19	0.99	–	0.23	Bal.
BS40–0.6Sn1.0Ti	256	285	40.09	1.03	0.65	0.19	Bal.

electron beam was moved in 0.2 μm steps over a 50 μm × 50 μm area.

3. Results and discussion

3.1. X-ray diffraction

The X-ray diffraction data for the raw powders and the SPS compacts of BS40–1.0Ti and BS40–0.6Sn1.0Ti are presented in Fig. 1. The raw powders were produced by the rapid solidification method. When cooled from the β field, the powders retained a single β′ phase state. For the BS40–1.0Ti SPS compacts prepared at 400 °C, α peaks appear at 32.324°, 49.52°, and 72.54°, which indicates that the α phase precipitates and parts of the β' phase are transformed to the α phase after exposure to thermal impact at 400 °C. The phase volume fractions of the α and β phases in the samples prepared at different temperatures are calculated using the XRD diffraction peak intensities [19], as shown in the following equation:

$$V_\alpha = \frac{I_{\alpha(1\,11)} + I_{\alpha(200)} + I_{\alpha(220)}}{I_{\alpha(111)} + I_{\alpha(200)} + I_{\alpha(220)} + I_{\beta(110)} + I_{\beta(200)} + I_{\beta(211)}} \times 100\% \quad (1)$$

where V_α is the α-phase volume fraction, I_α is the intensity of the α diffraction peak, and I_β is the intensity of the β diffraction peak. The α-phase ratio in the sintered BS40–0.6Sn1.0Ti compact increases from 50.5% to 52.3% when the temperature is increased from 400 °C to 500 °C, then decreases to 50.5% as the temperature is increased to 600 °C. For the sintered BS40–1.0Ti compact, the α-phase ratio shows a trend similar to that of the BS40–1.0Ti SPS compact. The α-phase ratio reaches a maximum value of 55.9% for BS40–1.0Ti and 52.3% for BS40–0.6Sn1.0Ti at 500 °C. The α-phase ratio reaches a maximum value at 500 °C with respect to the Cu–Zn binary phase diagram [7], which is consistent with that of the developed brasses in this study. The volume fraction of the β phase shows a corresponding balance variation with the volume fraction of the α-phase. A comparison of the materials shows that the α-phase volume fraction in the extruded BS40 is significantly higher: 82.6% at 400 °C, 84.9% at 500 °C and 80.8% at 600 °C. The addition of alloying elements changes the boundaries of the phase fields in the phase diagram as follows: an increase in the content of any additive other than Ni shifts the β-phase field toward low Zn content [20]. The shift of the maximum value of the α-phase ratio from 55.9% in BS40–1.0Ti to 52.3% in BS40–0.6Sn1.0Ti verifies that the addition of 0.6 wt% Sn is favorable to the formation of β-phase. Because the intermetallic β-phase exhibits greater hardness and better hot workability than the α-phase, the appropriate increment of the β-phase volume fraction created by the addition of Ti and Sn alloying elements is favorable to the mechanical properties of brass.

Minor peaks at 37.3°, 38.1° and 39.26° are also observed in the XRD patterns of the BS40–0.6Sn1.0Ti SPS compacts sintered at different temperatures, as shown in Fig. 1. These peaks are indexed by spacings that are characteristic of the ternary compound $CuSn_3Ti_5$. Two ternary compounds, $CuSn_3Ti_5$ and CuSnTi, and their crystal-structure data have been reported in the Cu–Sn–Ti system [14,15,18]. The ternary compound $CuSn_3Ti_5$ is in equilibrium with a liquid at 900 °C and evolves during cooling [14]. The peak intensity of $CuSn_3Ti_5$ increases with increased sintering temperatures, which indicates that the volume of $CuSn_3Ti_5$ increases with temperature from 400 °C to 600 °C.

3.2. Microstructure

The optical micrographs of the BS40–0.6Sn1.0Ti and BS40–1.0Ti SPS compacts sintered at different temperatures in the range of 400–600 °C are shown in Fig. 2(a)–(c) and (a′)–(c′), respectively. For comparison, the BS40 compacts prepared under the same conditions are shown in Fig. 2(a″)–(c″). The three raw powders prepared by water atomization consist of fundamentally equiaxial grains of

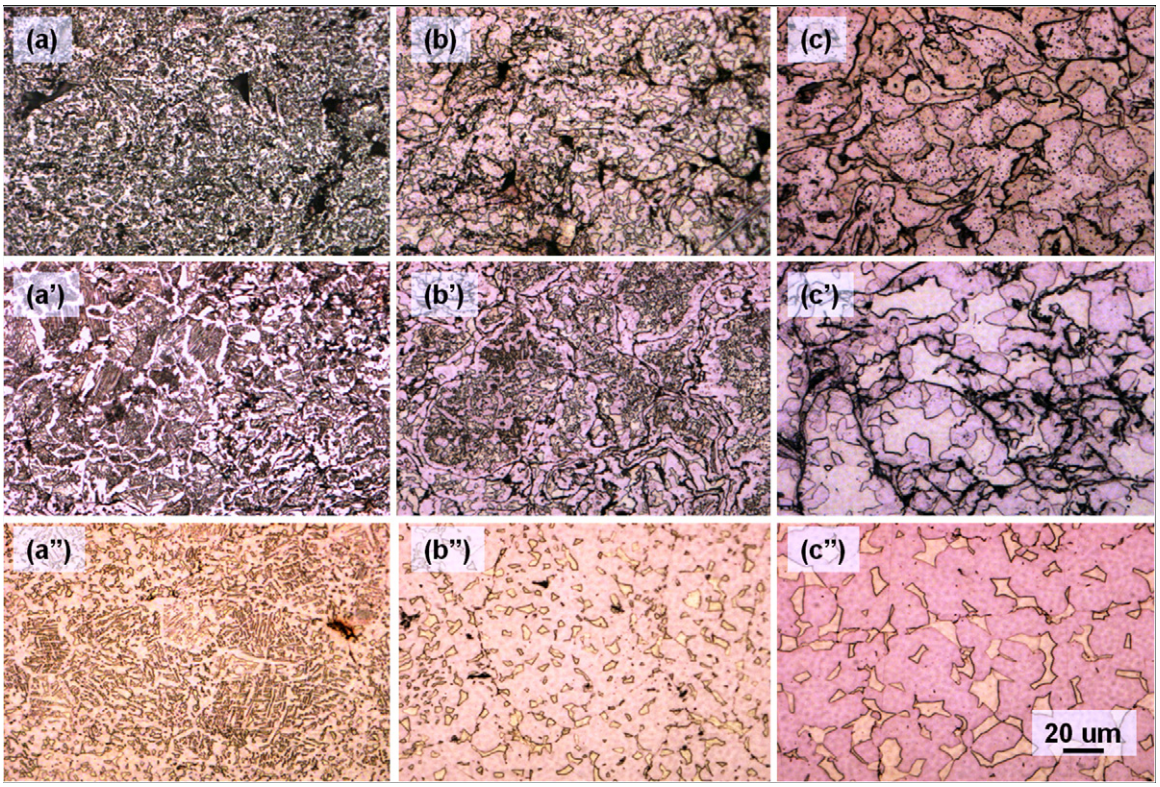

Fig. 2. Optical micrographs of BS40–0.6Sn1.0Ti at (a) 400 °C, (b) 500 °C, (c) 600 °C and BS40–1.0Ti at (a′) 400 °C, (b′) 500 °C, (c′) 600 °C; and BS40 (a″) 400 °C, (b″) 500 °C, (c″) 600 °C compacts prepared by SPS.

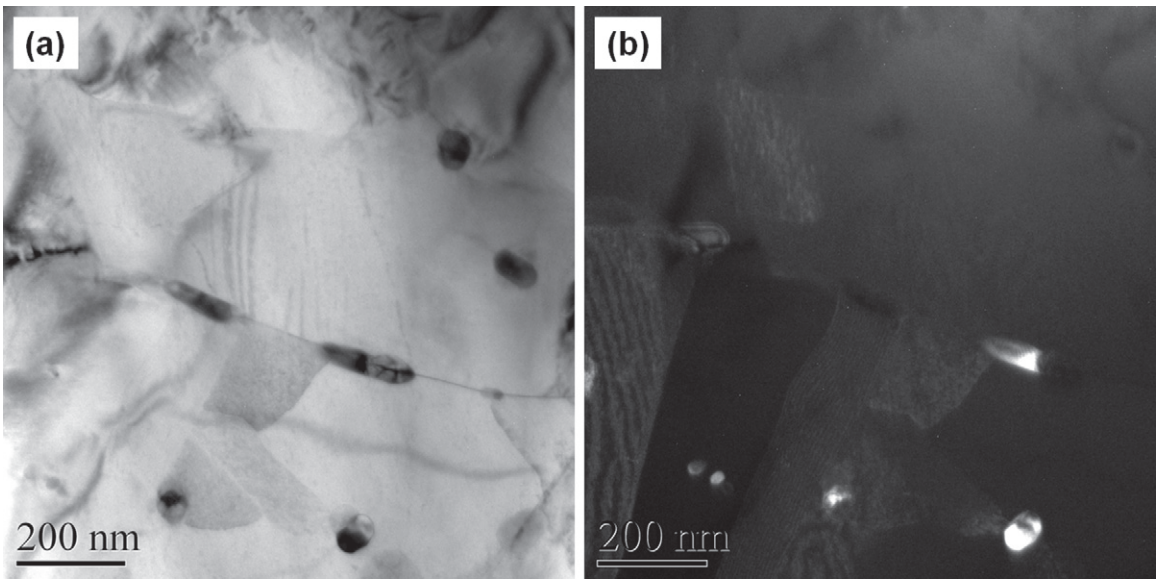

Fig. 3. Transmission electron micrographs of a BS40–0.6Sn1.0Ti SPS compact consolidated at 600 °C: (a) bright-field image and (b) dark-field image.

the β′ phase. After the samples were sintered at 400 °C for 1.8 ks, the α phase was observed to precipitate along the boundaries of the initial β′ phase, which is surrounded by the deeper-etching β′ phase. The α phase is visible as a fine laminar structure (a typical Widmanstätten structure) that emanates from the primary particle boundaries of the BS40–1.0Ti (Fig. 2(a′)) and BS40 (Fig. 2(a″)) compacts. The BS40–1.0Ti compacts exhibit a much finer morphology than the BS40 compact. Compared to that of BS40–1.0Ti compacts, BS40–0.6Sn1.0Ti shows notably finer grains than those of the binary alloy, as depicted in Fig. 2(a). In addition, fine precipitates are observed in both BS40–1.0Ti and BS-0.6Sn1.0Ti, distributed uniformly in their matrices. Because Sn addition causes no effective

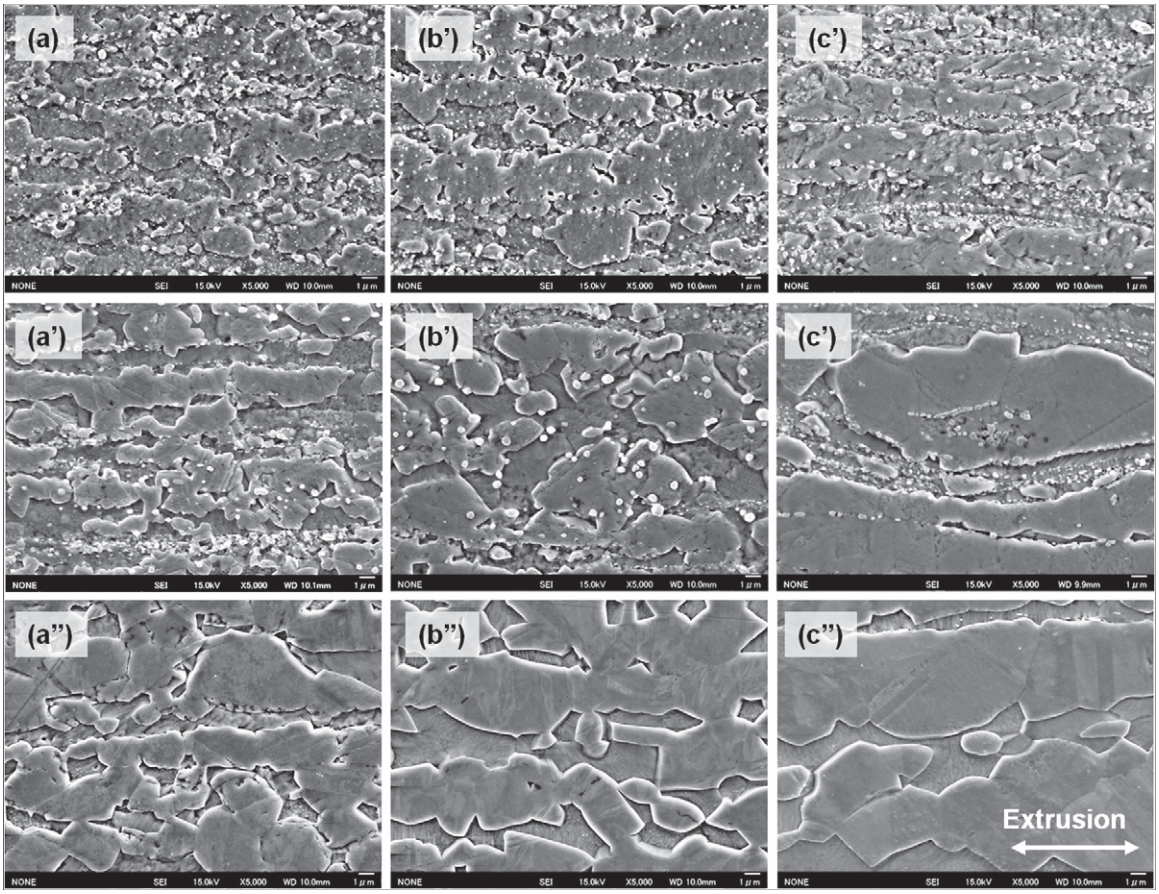

Fig. 4. SEM micrographs of the longitudinal cross-section of the extruded samples BS40–0.6Sn1.0Ti at (a) 400 °C, (b) 500 °C, (c) 600 °C; BS40–1.0Ti at (a′) 400 °C, (b′) 500 °C, (c′) 600 °C; and BS40 at (a″) 400 °C, (b″) 500 °C, (c″) 600 °C prepared by SPS.

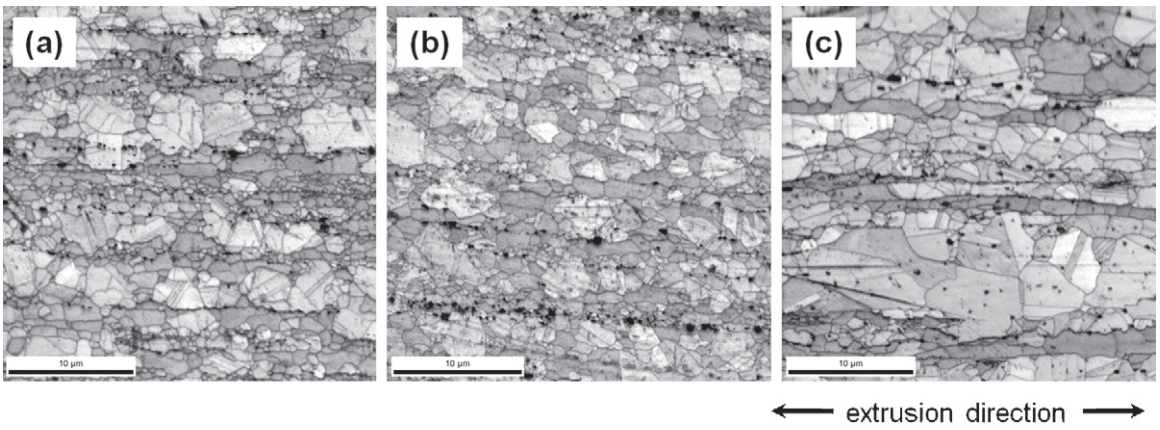

Fig. 5. The image-quality (IQ) map of the longitudinal cross-section of the extruded BS40–0.6Sn1.0Ti sintered at (a) 400 °C, (b) 500 °C, and (c) 600 °C by SPS.

grain refinement of yellow brass [21], Ti is identified as a beneficial element for grain refinement. The α and β phases gradually grow coarser with elevated temperature. The increased volume fraction of the α phase after sintering at 500 °C accompanies the coarser microstructure. The fine precipitates in both BS40–1.0Ti and BS40–0.6Sn1.0Ti grow coarser after sintering at 500 °C. The microstructure of the BS40–1.0Ti sintered at 600 °C (Fig. 2(c′)) exhibits a different morphology from that of the samples sintered at temperatures less than 600 °C. At this temperature, the α phase grows larger and develops an island shape in the β matrix. The Ti precipitate is completely concentrated in the primary particle boundaries when the temperature is increased to 600 °C. In contrast, BS40–0.6Sn1.0Ti exhibits a distinctly different morphology than BS40–1.0Ti: the Ti precipitates grow coarser, and the majority of the precipitates remain in the interior of the particles instead of concentrating in the primary particle boundaries after sintering at 600 °C (Fig. 2(c)). The precipitates are confirmed to be $CuSn_3Ti_5$ IMC according to their XRD pattern, as shown in Fig. 1. Fig. 3(a)–(b) shows the TEM micrographs of the BS40–0.6Sn1.0Ti SPS compact sintered at 400 °C. Ti precipitates with a size of 50 nm were observed in the interiors of the grains and at the grain boundaries, as shown in the bright field (BF) image in Fig. 3(a). These precipitates were also discernible in the dark-field (DF) image in Fig. 3(b).

Fig. 4 shows micrographs of the longitudinal cross-sections of the extruded BS40–0.6Sn1.0Ti, BS40–1.0Ti and BS40 consolidated at different temperatures. After extrusion with a reduction of 37%, the BS40–1.0Ti microstructure is characterized by a continuous α-phase elongation along the extrusion direction with corrugated boundaries and observable effects of plastic strain in the form of parallel intersection slip bands (Fig. 4(a′)–(c′)). At the lower sintering temperatures, such as 400 °C, the α phase consists of fine globules distributed along a different band after extrusion. The Ti precipitates assume the form of tiny second-phase particles dispersed uniformly throughout the microstructure (Fig. 4(a′)). Such a microstructure is expected to increase the mechanical properties of brass alloys. The morphology of the extruded sample sintered at 600 °C differs significantly from that of the samples sintered at lower temperatures (Fig. 4(c′)). The α phase becomes progressively coarse and elongates successively along the extrusion direction. The Ti precipitates distribute along the plastic flow line between the α/β-phase bands. This microstructure is explained by the tendency of Ti precipitates to segregate at the primary particle boundaries as the sintering temperature increases, which consequently weakens

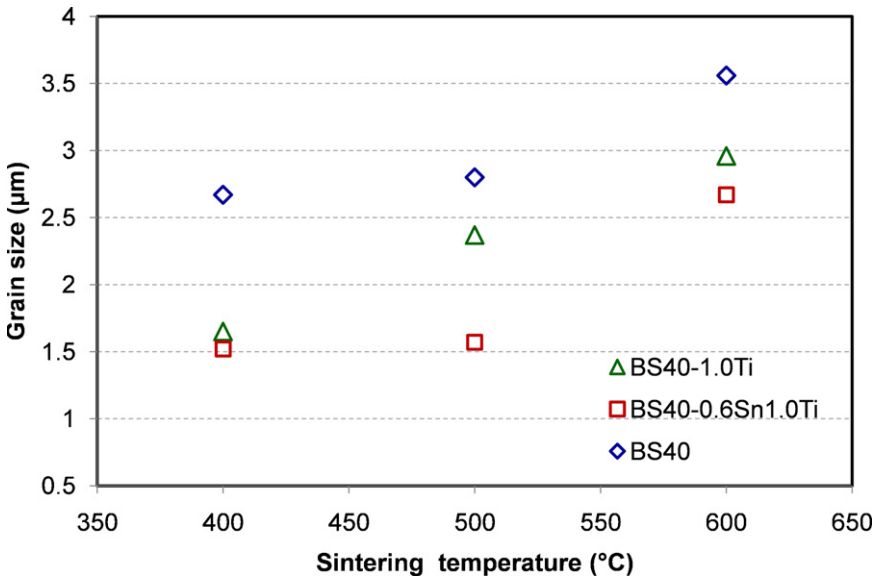

Fig. 6. The grain size in the longitudinal direction of the extruded BS40–0.6Sn1.0Ti, BS40–1.0Ti and BS40 as function of sintering temperature in the range of 400–600 °C.

Table 2
Mechanical properties of the extruded BS40, BS40–1.0Ti and BS40–0.6Sn1.0Ti brasses prepared using SPS in the temperature range of 400–600 °C.

Materials	Temp. (°C)	YS (MPa)	Deviation	UTS (MPa)	Deviation	Elongation (%)	Deviation
BS40	400	303.3	0.58	500.1	0.99	41.4	1.5
	500	288.0	1.66	493.7	0.27	39.7	3.76
	600	251.3	1.09	483.4	1.37	41.9	1.36
BS40–1.0Ti	400	390.2	12.94	617.0	12.55	26.6	2.72
	500	292.5	12.24	530.7	32.71	26.1	4.11
	600	247.8	11.27	498.6	34.42	26.5	2.62
BS40–0.6Sn1.0Ti	400	398.4	5.43	615.1	5.15	21.5	1.87
	500	355.2	24.84	601.4	27.98	21.9	2.45
	600	315.2	15.57	597.7	10.96	25.5	0.81

the constraint on the grain growth provided by the precipitates in the SPS compacts. The Ti precipitates are redistributed with the flow of the large plastic deformation of the soft brass matrix by the high extrusion pressure during the subsequent hot extrusion. Compared to BS40–1.0Ti, the BS40–0.6Sn1.0Ti exhibits a much finer morphology (Fig. 4(a)–(c)) in which ultrafine Ti precipitates are distributed uniformly throughout the structures, even at 600 °C. The finer microstructure of the BS40–0.6Sn1.0Ti is attributed to the uniform distribution of Ti precipitates in the matrix. After the addition of Sn, the segregation of Ti is inhibited by the formation of $CuSn_3Ti_5$ IMCs, which are retained in the interior of the particles instead of the particle boundaries at 600 °C. Consequently, the grain refinement effect is greatly intensified by the Ti precipitates.

Fig. 5 presents the image quality (IQ) map of the longitudinal cross-section micrographs of the extruded BS40–0.6Sn1.0Ti as detected by the electron backscatter diffraction (EBSD) technique. The grain boundaries are identified by lines, and the phase boundaries are identified by colors. The light-gray area represents the α-phase grains, and the dark-gray area represents the β-phase grains. After extrusion with a reduction of 37%, the BS40–0.6Sn1.0Ti microstructure is characterized by a discrete α phase distributed along the extrusion direction with corrugated boundaries (Fig. 5(a)). At the lower sintering temperatures, the α phase consists of fine globules distributed along a different band after extrusion. Recrystallization occurs in both the α phase and the β phase after hot extrusion, and the β phase exhibits a much finer grain size than the α phase. Twins can be observed in the α phase, which are a typical feature of dual brass. Grains in both the α and β phases grow moderately at 500 °C. The Ti precipitates (black dots) appear as tiny second particles that are not only dispersed along the plastic flow line between the α/β phase bands but also in the grain boundaries (Fig. 5(b)). The morphology of the extrusion sample sintered at 600 °C differs greatly from the morphologies of the samples sintered at lower temperatures. The α phase becomes progressively coarser and elongates successively along the extrusion direction (Fig. 5(c)).

The grain size in the longitudinal direction of the extruded samples is plotted in Fig. 6 as a function of the sintering temperature in the range of 400–600 °C. The extruded BS40–0.6Sn1.0Ti exhibited much smaller grain size than the extruded BS40–1.0Ti and BS40 at different sintering temperatures. From the longitudinal grain size of the extruded samples detected by EBSD, the relationship curves between the YS and the grain size (the so-called Hall–Petch relationship curves) are plotted in Fig. 7. The correlations between the YS and the grain size for the extruded BS40–1.0Ti and BS40 show good linear-fit relationships, which indicate ideal grain growth in both BS40–1.0Ti and BS40. However, the *R*-squared value for BS40–0.6Sn1.0Ti shows a slight deviation. Based on Fig. 5(a) and (b), grain growth is well restrained by the pinning effect of the fine Ti precipitates in the grain boundaries at 400 °C and 500 °C. Accompanying the reduction of the Ti precipitate population in the grain boundaries with increasing temperature, BS40–0.6Sn1.0Ti exhibits a quick grain growth at 600 °C, as shown in Fig. 5(c). Non-ideal grain growth occurs when grain growth is inhibited by the presence of a second phase that causes the growth to deviate from the ideal case. In comparison, BS40–1.0Ti exhibits a grain growth behavior similar to that of BS40 because the super-saturated Ti in BS40–1.0Ti segregates readily at primary particle boundaries at elevated temperatures. This segregation depresses the grain refinement effect. Based on these results, the deviation behavior of the grain growth in BS40–0.6Sn1.0Ti verifies that the addition of elemental Sn inhibits Ti segregation at high temperatures.

3.3. Mechanical properties

Fig. 8(a) shows the true stress versus true strain curves of the extruded BS40, BS40–1.0Ti and BS40–0.6Sn1.0Ti brasses, which are consolidated at different temperatures in the range of 400–600 °C. A photograph of the tensile sample used in the present study is presented in Fig. 8(a). All measurements of mechanical properties represent those of the extruded materials. The average values of the ultimate tensile strength (σ_{UTS}), the yield strength (σ_{YS}), and the elongation are summarized in Table 2. For the samples sintered at 400 °C, the σ_{UTS} of the BS40–1.0Ti is 617 MPa, which is 23.4% higher than that of the BS40 prepared under identical conditions. When the sintering temperature is increased from 400 °C to 600 °C, the σ_{UTS} is significantly reduced, decreasing by 19.2% from 617 MPa to 498 MPa, as shown in Fig. 8(b); this latter value is approximately the same as that of BS40 at 600 °C. The σ_{UTS} of the BS40–0.6Sn1.0Ti exhibits a distinctly different tendency than that of the BS40–1.0Ti. It has nearly the same σ_{UTS} value as the BS40–1.0Ti sintered at 400 °C, and it decreases by 2.8%, from 615 MPa to 598 MPa, when the sintering temperature is increased from 400 °C to 600 °C. These results indicate that the addition of elemental Sn has a significantly protective effect on the σ_{UTS} of BS40–0.6Sn1.0Ti at elevated temperatures.

Fig. 8(c) shows the effect of the sintering temperature on the 0.2% yield strength (σ_{YS}) of the three brasses. The values of σ_{YS} for all brasses decrease gradually when the sintering temperature is increased. BS40–1.0Ti and BS40–0.6Sn1.0Ti sintered at 400 °C have σ_{YS} values of 390 MPa and 392 MPa, which are 28.7% and 31.3% higher than the 303 MPa value of BS40, respectively. These results verify that the addition of Ti improves the yield strength of brass, while the addition of Sn does not. Interestingly, the behavior of BS40–1.0Ti is different from that of BS40–0.6Sn1.0Ti prepared at an elevated sintering temperature. The σ_{YS} of BS40–1.0Ti drops rapidly from 390 MPa to 248 MPa, losing 36.4% of its starting value, when the sintering temperature is increased from 400 °C to 600 °C. This result indicates that BS40–1.0Ti has approximately the same σ_{YS} value as that of BS40. In contrast, the σ_{YS} value of BS40–0.6Sn1.0Ti exhibits a moderate reduction of 20.8%. The decreased rate of σ_{YS} degradation at elevated temperatures is clearly attributable to the addition of Sn.

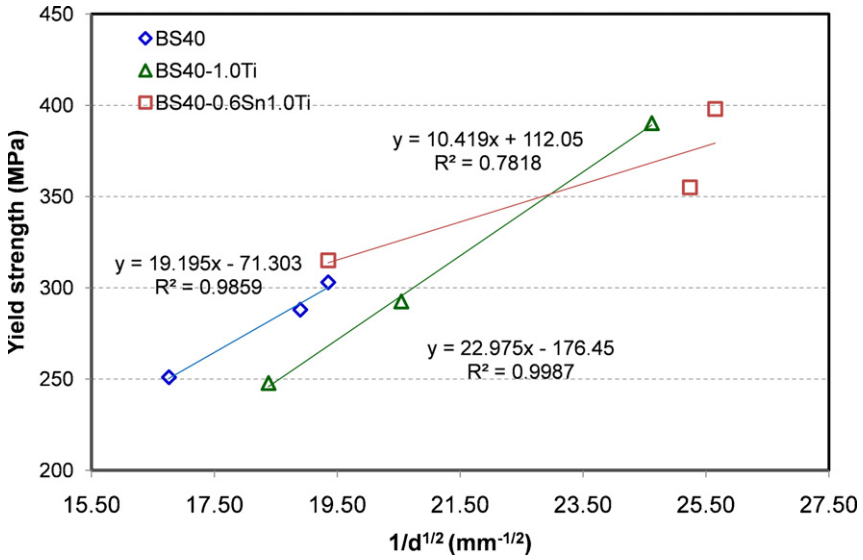

Fig. 7. The Hall–Petch relationship between the yield strength and the grain size in the longitudinal direction of the extruded BS40–0.6Sn1.0Ti, BS40–1.0Ti and BS40 at different sintering temperatures in the range of 400–600 °C.

Fig. 8(d) presents plots of the elongation versus sintering temperature for the three brasses. The addition of Ti adversely affects the ductility of BS40. The elongation of BS40–1.0Ti is 35.8% lower than that of BS40 at 400 °C. An increase in the sintering temperature shows little improvement on the ductility of either BS40 or BS40–1.0Ti. With regard to BS40–0.6Sn1.0Ti, the Ti and Sn additions induce a strong adverse effect on the ductility of BS40, which shows a 48.2% lower value than that of BS40 at 400 °C. However, the elongation of BS40–0.6Sn1.0Ti improves with elevated temperature. It exhibits approximately the same value as BS40–1.0Ti

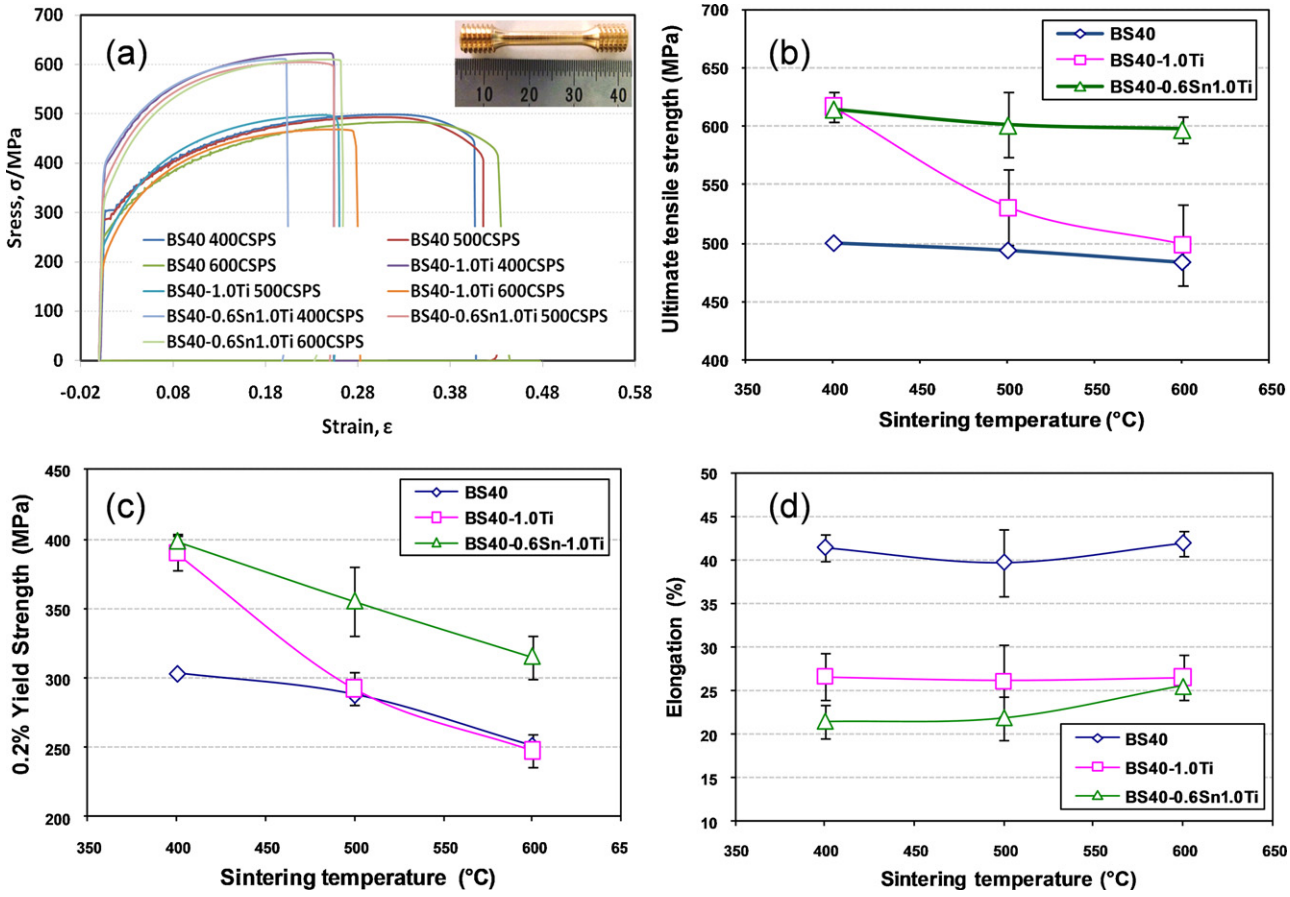

Fig. 8. Mechanical properties of the extruded BS40, BS40–1.0Ti and BS40–0.6Sn1.0Ti brasses; the billets are prepared by SPS at different temperatures in the range of 400–600 °C. (a) The true stress–strain curves of the extruded brasses. The inset shows a photograph of the tensile test sample. (b) Yield strength; (c) ultimate tensile strength; and (d) elongation of the extruded brasses as a function of sintering temperature.

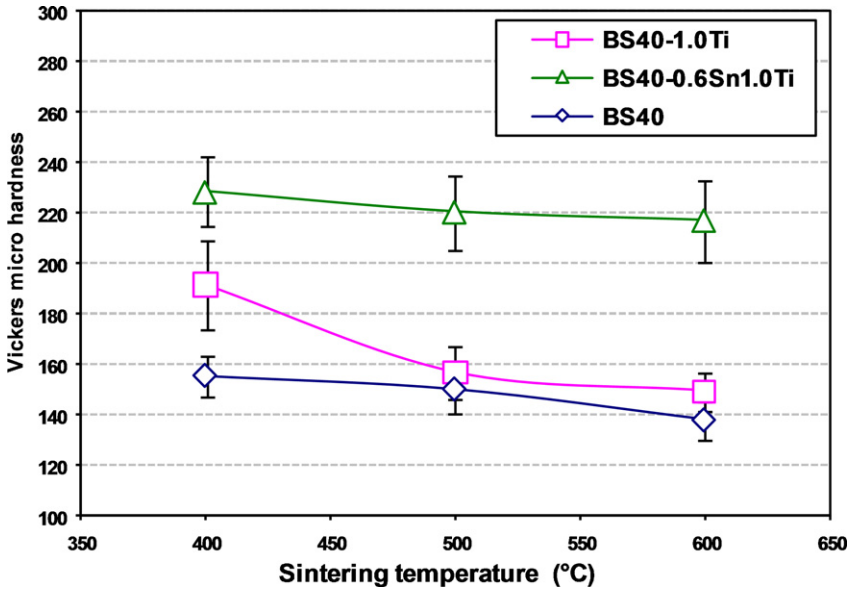

Fig. 9. Vickers micro-hardness of the extruded BS40, BS40–1.0Ti and BS40–0.6Sn1.0Ti brasses as a function of sintering temperature in the range of 400–600 °C.

at 600 °C, which is attributed to the impedance of Ti segregation at particle boundaries at high temperatures by added Sn, as shown in Fig. 8(c).

The decrease in the ductility after the addition of Ti and Sn is attributed to the segregation of the alloying elements in the grain boundaries; such imperfections always embrittle a material. The reduction of the ductile α-phase volume fraction is another essential factor. The α-phase ratio in BS40–0.6Sn1.0Ti is 52.3% at 500 °C, which is 38.4% lower than the 84.9% ratio in BS40. In addition, the elongation of BS40 decreases slightly at 500 °C instead of increasing concomitantly as the temperature increases. The ductile α-phase volume of BS40–0.6Sn1.0Ti increases to its maximum of 52.3% at 500 °C, as calculated using Eq. (1). This α-phase volume increase is presumably attributable to the variation of the chemical composition of the β phase, which exists as an intermetallic compound. The intermetallic β phase usually contains stoichiometric ratios of 45–49% Zn at 500 °C [2]. The increase of the Zn content in the β phase depresses its ductility because the α-phase volume ratio reaches a maximum value at 500 °C.

Fig. 9 shows plots of the Vickers micro-hardness versus the sintering temperature for the samples sintered at temperatures in the range of 400–600 °C. The hardness value of BS40–0.6Sn1.0Ti is 47.1% greater than that of BS40 at 400 °C; this result indicates the remarkable hardening effects of the addition of Ti and Sn. In addition, the hardness of both BS40–0.6Sn1.0Ti and BS40 decrease slightly with increasing sintering temperature. Only 5.3% of the hardness of BS40–0.6Sn1.0Ti is lost when the sintering temperature is increased from 400 °C to 600 °C. In contrast, the hardness of BS40–1.0Ti decreases sharply as the temperature is increased from 400 °C to 500 °C, and it exhibits approximately the same value as that of BS40 at 500 °C and 600 °C. These results verify that the segregation of Ti precipitates at the primary particle boundaries reduces the hardening effect imparted by the addition of Ti in BS40–1.0Ti. The results also verify that Sn addition effectively retains the hardening effect of BS40–1.0Ti at high temperatures. The often-reported variation in the hardness with different grain sizes is a result of the variation in the prior dislocation densities of the samples [22]. Variation in the dislocation densities of samples with different grain sizes may be a result of the method used for sample preparation. In solid mechanics, the material hardness is described as the resistance of a crystalline solid to deformation, which is inherently size-dependent over a scale that ranges from a fraction of a micron to approximately one hundred microns, in which smaller sized particles are harder [23]. In addition, the significant increase of the harder β-phase volume fraction produced by the Ti and Sn alloying elements is another essential factor that increases the hardness of BS40–0.6Sn1.0Ti.

3.4. Discussion

Encounters between dislocations and obstacles, such as grain boundaries, are known to impede dislocation motion, which causes the stress that is required for the deformation process to proceed increase [24]. Dislocations may be pinned by stress field interactions with other dislocation and solute particles or with physical barriers from grain boundaries and second precipitates. Rapid cooling rates retain the single β′ phase, and the super-saturated solid solution of 0.99 wt% Ti in the BS40–1.0Ti raw powder is formed. A high cooling rate can lead to the formation of a further refined microstructure, extend the solid solubility and even produce metastable phases [25,26]. One source of this size dependence is the presence of internal obstacles that restrict glide, such as incoherent precipitates, grain boundaries and phase boundaries; the obstacle leads to dislocation pile-ups that further restrict their motion. As a consequence, the mechanical properties increase as the scale of the microstructure decreases. The solid solubility of Ti in brass decreases rapidly with increasing heat-treatment temperature, as reported in our previous study [10]. Titanium addition causes a large precipitation–hardening response in 60/40 brass because the super-saturation of Ti in the 60/40 brass matrix creates a high degree of thermodynamic meta-stability. This meta-stability provides a high chemical potential for the precipitation reaction of Ti. The super-saturated solid solution of Ti results in strengthening of the solid-solution. Furthermore, precipitate strengthening derived from the fine precipitates causes significant grain refinement, which enhances the mechanical strength. As a result, BS40–1.0Ti exhibits significantly stronger mechanical properties than BS40 at low temperature. Unfortunately, Ti precipitates coalesce, coarsen, and segregate at the primary particle boundaries at higher temperatures. However, the possible recovery or dynamic recrystallization

induced by hot deformation at higher temperatures might reduce the dislocation density [27,28]. The recrystallization of the α phase that occurs during hot extrusion decreases the dislocation density, which strongly affects the mechanical behaviors of BS40–1.0Ti. The recrystallization therefore engenders the segregation of Ti precipitates at primary particle boundaries, which decreases the mechanical properties and hardness of the alloy. Consequently, the mechanical properties of BS40–1.0Ti continue to weaken as a result of the coarsening and clearing away of Ti precipitates in the primary particle boundaries at elevated temperatures.

Sun et al. [29] have established a model (SMJ model) for the nucleation of MnS particles near boundaries and dislocations in which all atoms in the boundaries and dislocations are presumed to be potential nucleation positions. This model can be used to interpret the precipitation mechanism of Ti in this study. The consumption of Cu and Zn atoms around an atom of Ti in boundaries or dislocations engenders the formation of nuclei and growth of Ti precipitates. The high-angle boundaries between the matrix grains act as rapid-diffusion channels at high temperature. These channels favor the coarsening of Ti precipitate particles in the boundaries, which weakens the pinning effects against boundary migration. According to the theory of precipitation hardening [30], a large number of nuclei appears in the matrix because of the severe driving force at the early aging stage, and the size of precipitated particles is small. The particles then grow with time, and the spacing between the precipitates becomes large. The precipitation and coarsening processes of the secondary phase are accompanied by the long-distance diffusion of the second-phase atoms. The evolution of the microstructures during the heat-treatment process causes the hardness of the materials to increase, then to decrease. Therefore, the mechanical properties continue to weaken as a result of the coarsening and clearing away of Ti precipitate particles in the BS40–1.0Ti alloy.

A super-saturated solid solution of 1.03 wt% Ti in BS40–0.6Sn1.0Ti raw powder is formed by the water-atomization method. The difference between the atomic radii of Ti, Sn, Cu, and Zn provides a strain field that favors the strengthening of the solid solution. Furthermore, rapid cooling from high temperatures applies stress that causes dislocation motion [31], thereby creating a high dislocation density and a high precipitation potential in the raw powder. The higher dislocation density of the microstructure provides more sites for precipitation, which generates a thermokinetic advantage for the precipitation reaction [32], and the super-saturated solution of Ti in the brass matrix creates a high chemical potential for the precipitation as well. The dislocation density increases gradually as the deformation strain increases during the hot extrusion, which supplies more potential nucleation sites for Ti precipitation. In fact, Ti precipitates in the form of an ultrafine dispersoid of $CuSn_3Ti_5$ with the addition of Sn during sintering. The precipitates distribute in grain boundaries and provide a pinning effect, which increases the resistance to grain boundary slip and produces marked work-hardening effects. However, the tiny $CuSn_3Ti_5$ precipitates induce significant refinement of the microstructure, which hinders the movement of dislocations so that stronger mechanical properties and higher hardness are achieved at lower sintering temperatures. The BS40–0.6Sn1.0Ti sintered at 600 °C exhibits a yield strength of 315 MPa, a tensile strength of 598 MPa and a micro-hardness of 216 Hv. These values are much higher than those of BS40–1.0Ti. These results show that the addition of Sn has remarkable positive effects on the alloy. Tin increases the hard strength by increasing the volume fraction of the harder β phase. Furthermore, it also can sustain the Ti precipitate strengthening by retaining the Ti precipitates in the interior of its grains and at grain boundaries in the form of $CuSn_3Ti_5$ IMC particles, as opposed to allowing them to segregate at the primary particle boundaries. For the development of high-strength brasses to satisfy the requirements of new applications during their service period, more detailed studies and systematic analyses must be undertaken to elucidate the interactions between the Ti and Sn alloying elements with respect to their precipitation behaviors, dynamic recrystallization, and segregation mechanisms in the brass matrix.

4. Conclusion

The addition of Ti and Sn alloying elements is found to increase the β phase volume fraction of 60/40 brass, which is favorable to its strength and hardness properties. The results of this study show that the super-saturated solid solution of Ti in the water-atomized 60/40 brass powder creates a high chemical potential for the precipitation reaction of the Ti. Remarkable grain-refinement and strengthening effects are achieved by the addition of Ti to 60/40 brass in the powder metallurgy route. However, Ti is found to be readily segregated in the primary particle boundaries at elevated temperatures, which significantly deteriorates the mechanical properties of the BS40–1.0Ti. To inhibit the segregation behavior of the Ti in the BS40–1.0Ti, Sn is proposed as an additive. The Ti precipitates in the form of $CuSn_3Ti_5$ in grain boundaries, rather than segregating at the primary particle boundaries; this result leads to significant grain refinement and mechanical strengthening effects on the BS40–0.6Sn1.0Ti brass. These results show that the introduction of Sn to BS40–1.0Ti brass can effectively impede the segregation of Ti and stabilize the mechanical properties at high processing temperatures via powder metallurgy.

Acknowledgments

This work was supported as a project of the Japan Science and Technology Agency (JST). The authors sincerely thank the researchers of the Joining and Welding Research Institute (JWRI) at Osaka University as well as Mr. Yoshinori Muraki and Mr. Kyugo Inui for assistance in carrying out the extrusion experiments and tensile tests.

References

[1] J.R. Davis, Alloying, Understanding the Basics, ASM International, Materials Park, OH 44073-0002, 2001.
[2] J.R. Davis, Copper and copper alloys, in: Handbook Committee, ASM International, Materials Park, OH 44073-0002, 2001.
[3] E.G. West, Copper and its Alloys, Ellis Horwood Ltd., 1982.
[4] S. Li, H. Imai, H. Atsumi, K. Kondoh, J. Alloys Compd. 493 (2010) 128–133.
[5] S.V. Smirnov, N.B. Pugacheva, A.N. Soloshenko, A.V. Tropotov, Phys. Met. Metallogr. 93 (2002) 584–593.
[6] T. Nakagawa, T. Tanaka, T. Amano, J. Mech. Working Technol. 2 (1978) 179–195.
[7] Metals Handbook, Alloy Phase Diagrams, ASM Handbook, vol. 3, 10th ed., 1990.
[8] K.C.H. Kumar, I. Ansara, P. Wollants, L. Delaey, Z. Metallkunde 87 (1996) 666–672.
[9] S. Li, H. Imai, H. Atsumi, K. Kondoh, J. Mater. Sci. 45 (2010) 5669–5675.
[10] S. Li, H. Imai, H. Atsumi, K. Kondoh, Mater. Des. 32 (2011) 192–197.
[11] S. Li, H. Imai, A. Kojima, Y. Kosaka, K. Yamamoto, M. Takahashi, H. Atsumi, K. Kondoh, Adv. Mater. Res. 233–235 (2011) 2732–2735.
[12] W.A. Soffa, D.E. Laughlin, Prog. Mater. Sci. 49 (2004) 347–366.
[13] A. Poter, A.W. Thompson, Scripta Metall. 18 (1984) 1185–1188.
[14] S. Nagarjuna, K. Balasubramanian, D.S. Sarma, J. Mater. Sci. 34 (1999) 2929–2942.
[15] C. Kuper, W. Peng, A. Pisch, F. Goesmann, R. Schmidht-Feetzer, Z. Metallkde 89 (1998) 855.
[16] N. Saunders, A.P. Miodownik, Bull. Alloy Phase Diagrams 11 (1990) 278–287.
[17] S. Hamar-Thibault, C.H. Allibert, J. Alloys Compd. 317–318 (2001) 363–366.
[18] X. Zhang, Y. Zhan, Q. Guo, G. Zhang, J. Hu, J. Alloys Compd. 480 (2009) 382–385.
[19] G. Chu, Y.F. Cong, H.J. You, ACTA Metall. Sin. (English) 16 (2003) 489–494.
[20] N.B. Pugacheva, A.A. Pankratov, N. Yu Frolova, I.V. Kotlyarov, Russ. Metall. 3 (2006) 239–248.
[21] M. Sadayappan, J.P. Thomson, M. Elboujdaini, G. Ping Gu, and M. Sahoo, MTL Report 6 (2004) (TR-R).
[22] L.Y. Yee, C.M. Munawar, Philos. Mag. A 82 (2002) 2071–2080.
[23] L.Y. Zhang, Y.H. Jiang, Z. Ma, S.F. Shan, Y.Z. Jia, C.Z. Fan, W.K. Wang, J. Mater. Proc. Technol. 207 (2008) 107–111.

[24] E.O. Hall, Proc. Phys. Soc. B 64 (1951) 747–753.
[25] H. Jones, Mater. Lett. 26 (1996) 133–136.
[26] L. Katgerman, F. Dom, Mater. Sci. Eng. A 375–377 (2004) 1212–1216.
[27] W. Mao, Z. An, Y. Li, Frontiers Mater. Sci. China 2 (2008) 233.
[28] W. Mao, Z. An, W. Guo, P. Yang, Steel Res. Int. 81 (2010) 6.
[29] W.P. Sun, M. Militzer, J.J. Jonas, Metall. Trans. 23A (1992) 821–830.
[30] D.A. Porter, K.E. Esterling, Phase Transformations in Metals and Alloys, Van Nostrand Reinhold Company Ltd., 1981.
[31] J.W. Hall, H.F. Rase, I & EC Fundamentals 3 (1964) 158–167.
[32] H. Fernee, J. Nairn, A. Atrens, J. Mater. Sci. 36 (2001) 5497–5510.